Title
Mechanisms of Sinoatrial Node Dysfunction in Heart Failure With Preserved Ejection Fraction

Journal
Circulation, 145(1)

ISSN
0009-7322

Authors
Mesquita, Thassio
Zhang, Rui
Cho, Jae Hyung
et al.

Publication Date
2022-01-04

DOI
10.1161/circulationaha.121.054976

Peer reviewed

HHS Public Access

Author manuscript

Circulation. Author manuscript; available in PMC 2022 May 09.

Published in final edited form as:

Circulation. 2022 January 04; 145(1): 45–60. doi:10.1161/CIRCULATIONAHA.121.054976.

Mechanisms of Sinoatrial Node Dysfunction in Heart Failure with Preserved Ejection Fraction

Thassio Mesquita, PhD[1,*], **Rui Zhang, MD**[1,*], **Jae Hyung Cho, MD, PhD**[1,*], **Rui Zhang, MD**[1], **Yen-Nien Lin, MD, PhD**[1], **Lizbeth Sanchez, BS**[1], **Joshua Goldhaber, MD**[1], **Joseph K. Yu, BS**[2], **Jialiu A. Liang, BS**[2], **Weixin Liu, BS**[1], **Natalia A. Trayanova, PhD**[2,3], **Eugenio Cingolani, MD**[1]

[1]Smidt Heart Institute, Cedars-Sinai Medical Center, Los Angeles, California, USA.

[2]Department of Biomedical Engineering, Johns Hopkins University, Baltimore, Maryland.

[3]Alliance for Cardiovascular and Diagnostic and treatment Innovation (ADVANCE), Johns Hopkins University, Baltimore, Maryland.

Abstract

Background: The ability to increase heart rate (HR) during exercise and other stressors is a key homeostatic feature of the sinoatrial node (SAN). When the physiologic HR response is blunted, chronotropic incompetence limits exercise capacity, a common problem in patients with heart failure (HF) and preserved ejection fraction (HFpEF). Despite its clinical relevance, the mechanisms of chronotropic incompetence remain unknown.

Methods: Dahl salt-sensitive rats fed with a high-salt diet and C57Bl6 mice fed with high fat and an inhibitor of constitutive nitric oxide synthase (L-NAME, 2-hit) were used as models of HFpEF. Myocardial infarction was created to induce HF with reduced ejection fraction (HFrEF). Rats and mice fed with a normal diet or having a sham surgery served as respective controls. A comprehensive characterization of SAN function and chronotropic response was conducted by *in vivo*, *ex vivo*, and single-cell electrophysiological studies. RNA sequencing of SAN was performed to identify transcriptomic changes. Computational modeling of biophysically-detailed human HFpEF SAN was created.

Results: Rats with phenotypically-verified HFpEF exhibited limited chronotropic response associated with intrinsic SAN dysfunction, including impaired β-adrenergic responsiveness and an alternating leading pacemaker within the SAN. Prolonged SAN recovery time and reduced SAN sensitivity to isoproterenol were confirmed in the 2-hit mouse model. Adenosine challenge unmasked conduction blocks within the SAN, which were associated with structural remodeling.

Address correspondence to: Eugenio Cingolani, MD, Smidt Heart Institute, Cedars-Sinai Medical Center, 127 S. San Vicente Blvd., Los Angeles, CA 90048, eugenio.cingolani@csmc.edu.

*These authors equally contributed to this work

DISCLOSURES

None

Supplemental Materials

Expanded Methods

Supplemental Figures I – XV

Supplemental Tables I – IX

Supplemental Movies I – IV

References 58–62

Chronotropic incompetence and SAN dysfunction were also found in HFrEF rats. Single-cell studies and transcriptomic profiling revealed HFpEF-related alterations in both the “membrane clock” (ion channels) and the “Ca^{2+} clock” (spontaneous Ca^{2+} release events). The physiological impairments were reproduced *in silico* by empirically-constrained quantitative modeling of human SAN function.

Conclusions: Thus, chronotropic incompetence and SAN dysfunction were seen in both models of HF. We identified that intrinsic abnormalities of SAN structure and function underlie the chronotropic response in HFpEF.

Keywords

heart failure; sinoatrial node; chronotropic incompetence; arrhythmias

Introduction

The positive chronotropic effect of β-adrenergic receptor (β-AR) stimulation on the heart is a physiological response experienced during emotional and physical stressors. Impaired heart rate (HR) response to acute stress (also known as the fight-or-flight response) is manifested in patients with chronotropic incompetence (CI), which has been associated with adverse outcomes and increased mortality in heart failure (HF) with preserved ejection fraction (HFpEF)[1,2]. However, the mechanisms responsible for CI in HFpEF remain unclear. Impaired sinoatrial node (SAN) function has been posited in patients with HFpEF[3], but others implicate extrinsic factors (limited biventricular compliance[4], impaired vasodilation[1], elevated pulmonary pressure[5], and other peripheral and autonomic abnormalities[6]). SAN dysfunction has been extensively studied in other diseases[7,8], including chronic HF with reduced ejection fraction (HFrEF)[9,10], establishing the foundation for theories on the mechanisms of SAN arrhythmias[7,11]. Moreover, SAN dysfunction facilitates the development of atrial fibrillation[12], a rhythm disorder associated with HFpEF[13].

We therefore hypothesize that SAN dysfunction underlies the CI in HFpEF. To investigate the role of the intrinsic pacemaker on CI in HFpEF, we performed extensive SAN phenotyping (both at baseline and after stress) in the well-characterized Dahl salt-sensitive (DSS) rat model of HFpEF. This model has features reminiscent of human HFpEF: 1) signs of HF, with no decline in global systolic function[14]; 2) comorbidities including hypertension, insulin resistance, and hyperlipidemia[15,16]; and 3) adverse electrical remodeling with a high incidence of sudden death[17,18]. Given the heterogeneity of HFpEF sub-phenotypes and the variety of comorbidities in human HFpEF, the main findings were validated in the 2-hit HFpEF mouse model[19–21].

Methods

The data, analytical methods, and study materials will be made available to other researchers for purposes of reproducing results or replicating the procedures by reasonable request directed to the corresponding author. Descriptions and sources of reagents and detailed methods are provided in the Online Supplement Materials. All animal procedures were

reviewed and approved by the Institutional Animal Care and Use Committee of Cedars-Sinai Medical Center.

Statistical analysis

Pooled data are expressed as mean ± standard error of mean (SEM). Statistical comparisons were performed using GraphPad Prism 9 (San Diego, CA, USA). Differences between groups were tested using a two-tailed unpaired Student's t-test, or where repeated measures (RM), either RM-ANOVA or mixed-effect model when missing data occurred. Post-hoc pairwise testing was Bonferroni corrected for multiple comparisons. Proportions were tested using Fisher's exact test. Kaplan-Meier analysis was used for survival rates with the log-rank test. A p-value <0.05 was considered statistically significant.

Results

Exercise intolerance and chronotropic incompetence of HFpEF are associated with lower β-AR responsiveness

Dahl salt-sensitive (DSS) rats fed a high-salt (HS) diet develop phenotypic changes of HFpEF[17]. The experimental timeline is shown in Figure 1A. All animals underwent initial screening by echocardiography (Online Table I). Between 14–18 weeks (Figure 1B), ejection fraction (EF) remained unchanged in HS-fed DSS rats compared to those fed a normal-salt (NS) diet (control). In contrast, analysis of E and A-wave from pulse-wave Doppler mode, and E' and A'-wave changes in tissue Doppler, showed diastolic dysfunction as evidenced by decreased E/A ratio (Figure 1C) and increased E/E′ ratio (Figure 1D). Hypertension, which is one of the most prevalent comorbidities in human HFpEF[2], was developed in HS-fed DSS animals (Figure 1E). Importantly, HS-fed DSS animals exhibited the following HF signs: weakness, decreased mobility, labored breathing, and/or body edema, as represented by the elevated HF score in Figure 1F. Rats with HF signs and echo-verified diastolic dysfunction (and preserved EF) were diagnosed with HFpEF and used for the following experiments. Pulmonary congestion was verified by increased lung weight to tibia length (LW/TL) ratio in HFpEF animals compared to controls (Online Figure I).

In order to assess the chronotropic reserve, we used cardiopulmonary exercise stress testing. Despite no changes in baseline HR, at maximal exercise capacity, all animals presented an increase in HR (Figure 1G–H). However, HFpEF animals showed a significantly smaller increase in the maximal HR compared to control animals (Figure 1G–H), indicative of CI. Exercise intolerance was observed in our HFpEF animals (Figure 1H, inset), as also described in HFpEF patients[1]. Although the reduced functional capacity may limit the maximal HR response to exercise (Figure 1I), impaired HR regulation may also occur after exercise cessation[22]. In control animals, typical post-exercise HR recovery was shown with two distinct phases: (1) a fast phase, characterized by exponential HR recovery, mainly due to parasympathetic reactivation, followed by (2) a slow component, characterized by a gradual decay of HR as the result of the sympathetic withdrawal (Figure 1J). However, the prolonged HR recovery after exercise in HFpEF revealed two sub-types of CI: (1) submaximal peak of HR (Figure 1G–H), and (2) inadequate HR recovery (Figure 1J). To

exclude potential interference of limited functional capacity in HFpEF animals from the chronotropic response, we carried out an *in vivo* pharmacological stimulation test with isoproterenol, a non-selective agonist of β-AR (Figure 1K). Validating our exercise findings, HFpEF animals had a lower chronotropic response to β-AR stimulation compared to controls (Figure 1L–M). To study the potential impact of chronotropic response on cardiac output (CO), we performed a dobutamine stress-echocardiogram on control and HFpEF rats. Importantly, HFpEF rats presented inadequate CO reserve in response to dobutamine infusion (Online Figure II).

Given the heterogeneity of HFpEF subphenotypes, we also conducted experiments using the recently described 2-hit mouse model[19]. Mice concomitantly fed with a high-fat diet (metabolic hit) and nitric oxide synthase inhibitor (hypertensive hit) manifested increased left ventricular filling pressures and preserved EF as measured by noninvasive echocardiogram (Online Figure III, A–D and Online Table II), elevated systemic blood pressure (Online Figure III, E), and increased LW/TL (Online Figure III, F). Although no statistical differences were seen at baseline or maximal HR in HFpEF mice compared to controls, the fractional increase in HR in HFpEF mice was significantly smaller (Online Figure III, G). Limited exercise tolerance (Online Figure IIIG, inset) and delayed post-exercise HR recovery (Online Figure III, H) were also seen in HFpEF animals. Together, our findings in two different models of HFpEF demonstrated exercise intolerance and limited chronotropic response, mirroring the clinical features of human HFpEF. Although both HFpEF models showed an inadequate CO response to dobutamine (Online Figure IV), the impaired chronotropic response was the major driver in DSS HFpEF rats (Online Figure II), while a marginal increase in stroke volume appeared to be the main factor in HFpEF mice (Online Figure IV).

To elucidate if our findings were unique to HFpEF, we characterize them in a previously established model of HFrEF[9]. Rats with characteristic signs of HF and reduced EF (<45%) were referred to as HFrEF (Online Figure V, A–C), and compared to controls (Online Table III). Despite the significant change in absolute HR in response to exercise in HFrEF compared to controls (Online Figure V, D), the fractional increase was similar between groups. HFrEF rats also presented reduced exercise capacity (Online Figure V, D inset) and delayed post-exercise HR recovery (Online Figure V, E). Accordingly, as previously seen in HFrEF patients[10], cSNRT was prolonged in HFrEF rats compared to controls (Online Figure V, F). Moreover, limited chronotropic response to *in vivo* β-AR stimulation was observed in HFrEF rats (Online Figure V, G). In summary, most of the functional changes in SAN function and exercise capacity observed in both models of HFpEF were not exclusive of this condition, and were also seen in rats with HFrEF.

Impaired SAN β-AR responsiveness reveals uncoordinated recruitment of pacemaker clusters favoring rhythmic abnormalities

Autonomic imbalance, contributing to impaired chronotropic response, has been described in human HFpEF[1]. To exclude a contribution from autonomic innervation *in vivo*, we optically mapped intact SAN/atrial preparation *ex vivo*. Figure 2A shows that the functional and anatomical boundaries of the rat SAN are similar to those of the human SAN[23].

Representative activation maps demonstrate that, under spontaneous sinus rhythm, the earliest activation site is located at the right atrial posterior wall, which anatomically corresponds to the location of the SAN (Figure 2A). In concordance with our *in vivo* findings (Figure 1K–M), a blunted beating rate response to β-AR stimulation was also evident in isolated SAN tissue from HFpEF rats compared to controls (Figure 2B). Given the fact that β-AR isoforms and G protein-coupled receptor kinases (GRK) work in concert to desensitize, internalize, and ultimately downregulate β-AR in HFrEF ventricular myocardium[24], we next evaluated the abundance of these key proteins in the SAN. Neither mRNA nor protein expression of β-AR isoforms (β_1 and β_2) was changed in the SAN of HFpEF rats compared to controls (Online Figure VI, A–B). Moreover, no significant changes were observed in the protein expression of cardiac isoforms of GRKs (GRK2 and GRK5) or phosphorylation levels in the activating site of $GRK2^{ser670}$ (Online Figure VI, B). In accordance with the rat HFpEF model, atrial/SAN preparation from phenotypically verified 2-hit HFpEF mice presented an attenuated beating rate in response to isoproterenol (Online Figure VII, A) compared to control. The presence of an oscillatory leading pacemaker site (Online Figure VII, B and Online Video I), irregular beating rate, and conduction blocks were also observed (Online Figure VII, C).

To functionally characterize the activation pattern of the SAN in both experimental groups, high-resolution optical mapping was performed (Figure 2C). Although one control SAN preparation displayed two competing activation sites, the remaining samples had a single and coordinated leading pacemaker focus. β-AR stimulation slightly shifted the leading pacemaker towards the superior aspect within the SAN area. Conversely, even at baseline, multiple and disorganized leading pacemaker sites were observed in HFpEF SAN preparations, while β-AR stimulation failed to shift and resynchronize the leading pacemakers (Figure 2C). In concordance with the chaotic activation pattern, 85% of HFpEF SAN preparations developed irregular rhythms (e.g., atrial bigeminy, sinus arrest, tachy-bradycardia, and atrial fibrillation) upon isoproterenol stimulation identified by field atrial/SAN electrogram (Figure 2D). By contrast, only one control SAN preparation displayed a brief bigeminy episode, while most of the controls sustained high beating rates under coordinated sinus rhythm (Figure 2D).

The SAN is almost entirely insulated from the surrounding atria by fibrosis, fat, and discontinuous myofibers[25]. Masson's trichrome staining distinguished the SAN region surrounding the SAN artery from the neighboring atria (Figure 2E). Increased SAN fibrosis was observed in HFpEF SAN compared with controls (Figure 2E). Although fibrotic remodeling of SAN can impact electric conduction[26], no significant change in conduction velocity within the SAN region was observed between groups at baseline (Figure 2F). However, following β-AR stimulation, a dose-dependent increase in beating rate, supported by faster electrical impulse propagation, was seen in controls, but not in HFpEF SAN preparations (Figure 2F). Taken together, we show that impaired chronotropic response is associated with the presence of multiple intranodal pacemakers, revealing a distinctive pattern of intrinsic SAN dysfunction in HFpEF.

Adenosine challenge reveals areas of SAN exit block

Intracardiac programmed electrical stimulation was used to measure the corrected SAN recovery time (cSNRT) as a measure of *in vivo* SAN function (Figure 3A–B). Supporting our hypothesis of impaired SAN function, Figure 3C shows prolonged cSNRT in HFpEF animals compared to controls. Circadian HR oscillation shows similar diurnal variation, and narrower heart rate variability during the nocturnal period in HFpEF compared to control animals (Figure 3D), supporting autonomic dysfunction previously reported in both humans and animal models[1,18]. While these HFpEF changes are associated with higher mortality (Figure 3E), it is important to point out that the overall mortality reported here includes not only sudden death (as we previously reported[18]), but also those following the protocol-mandated euthanasia criteria due to severe distress of the animals[27].

Given the previous results, we then tested the SAN function in an intact *ex vivo* atrial/SAN preparation[23]. Optical maps during pacing-induced suppression of sinus rhythm led us to identify areas of dysfunction within the SAN and the presence of conduction blocks. Substantiating our *in vivo* findings, we also found longer cSNRT in HFpEF SAN compared to controls (Figure 3F). In concordance with our findings in the DSS rat HFpEF model, atrial/SAN preparation from 2-hit HFpEF mice presented longer cSNRT compared to controls (Online Figure VII, D). We further stressed the rat SAN by exposure to adenosine (1 μM, as complete SAN arrest can be seen at higher concentrations[23]). As expected, adenosine-induced suppression of SAN automaticity was observed by a reduction of the intrinsic beating rate in both groups. However, cSNRT was longer in HFpEF, while remaining unchanged in control SAN tissue (Figure 3F). Using our integrated mapping approach, we mapped several regions of SAN conduction pathways responsible for the conductibility of electrical impulses to the right and left atria[7,23,28]. Interestingly, no conduction block was detected in control samples exposed to adenosine. On the other hand, an interatrial block was observed in 67% of HFpEF samples (Figure 3G). Thus, these results indicate that HFpEF animals have a vulnerable SAN fail-safe mechanism for automaticity and conduction in response to stressors.

Suppressed membrane clock in HFpEF SAN

To explore the molecular basis of the SAN dysfunction in HFpEF rats, we performed next-generation RNA sequencing in isolated SAN tissue. SAN-specificity was verified by sequencing SAN and atrial tissue from control rats. Accordingly, control SAN tissue presented higher levels of *Hcn4*, *Shox2*, and *Tbx3* compared to atrial tissue (Online Figure VIII, A), confirming enriched molecular markers of SAN. RNA-seq revealed changes in the expression of 835 genes in HFpEF SAN compared to controls (635 upregulated and 200 downregulated, Online Table IV). Taking into consideration recent studies profiling the molecular signatures of different cell types that populate the SAN at the embryonic stage[29,30], we only observed a significant loss of *Igfbp5* and *Hcn4* (belonging to compact SAN) in HFpEF SAN, without enrichment of transitional/atrial-like genes (Online Figure VIII, B). Thus, these findings do not indicate a molecular shift towards a less nodal phenotype in SAN of HFpEF animals.

Ingenuity Pathway Analysis (IPA) was performed to investigate the upregulated and downregulated canonical pathways (Figure 4A, Online Table V). Along with these findings, gene ontology analysis revealed that SAN dysfunction in HFpEF animals was associated with significant enhancement of multiple disease-associated genes, including inflammation, extracellular matrix remodeling, and metabolic pathways (Online Table VI). To verify whether the transcriptome changes align with the available human database, further IPA *in silico* analysis was used. By objectively filtering our analysis to the tissue type and disease, the closest related disease to SAN dysfunction was sick sinus syndrome. As highlighted in the volcano plot, among the five potential genes related to human sick sinus syndrome (*Hcn4*, *Cacna1d*, *Myh6*, *Snta1*, and *Scn5a*), two of them (*Hcn4* and *Cacna1d*) were significantly downregulated in HFpEF SAN transcriptome compared to control samples (Figure 4B). A comprehensive representation of differential expression of membrane and Ca^{2+} clock genes in HFpEF SAN is presented in Online Figure IX. RNA sequencing data have been deposited in the National Center for Biotechnology Information's Gene Expression Omnibus under accession number GSE184120.

Next, we probed selected proteins to validate our RNA-seq data. In agreement, we found a decrease in protein levels of $Ca_v1.3$ (encoded by *Cacna1d* gene) (Figure 4C). To assess the functional implications of these findings, we then assessed the Ca^{2+} current in isolated SAN cells, which revealed typical spindle-shaped morphology of pacemaker cells with absent (or poorly present) t-tubules (Figure 4D). We consistently observed reduced L-type Ca^{2+} currents in HFpEF cells compared to controls (Figure 4E and G). No changes in cell capacitance were observed between groups (Figure 4F). Although two distinct L-type Ca^{2+} channels are expressed in the SAN: $Ca_v1.2$ (encoded by *Cacna1c* gene) and $Ca_v1.3$, the latter being the most predominant isoform in SAN cells[31], $Ca_v1.2$ expression remained unchanged between groups (Online Figure X, C). The contribution of T-type Ca^{2+} channels, mainly $Ca_v3.1$ (encoded by *Cacna1h*), has also been demonstrated in pacemaker cells[32]. In our study, we found $Ca_v3.1$ expression in SAN tissue (Online Figure X, A) and patch-clamp studies carried out in control SAN cells revealed an expected leftward shift of current-voltage relationship, peaking at a more hyperpolarized voltage (−30 mV) compared to LTCC (peak at 0 mV) (Online Figure X, B). Interestingly, T-type Ca^{2+} current density was 23-fold smaller than L-type, thereby indicating a minor contribution of T-type Ca^{2+} current in rat pacemaker cells, as also described in different species[33]. To obtain insights into the contribution of L-type Ca^{2+} channels to the lower chronotropic reserve of HFpEF rats, we stimulated SAN cells with isoproterenol (1 μM). Although the peak current in HFpEF SAN cells (after isoproterenol stimulation) was smaller than in controls, the fractional increase of Ca^{2+} current upon isoproterenol stimulation was similar between groups (Figure 4H). Despite these changes, the maximal diastolic membrane potential remained unchanged between groups (Online Figure XI).

Hcn4 is another critical component of the pacemaker function and is indicated as a potential player in the SAN dysfunction in HFpEF animals. As shown in Figure 4I, a decrease in the Hcn4 protein content of SAN from HFpEF compared to control largely correlated with the dramatic reduction in whole-cell I_f conductance (Figure 4J–K). No changes were observed at relevant diastolic membrane potentials (−60 to −30 mV, Figure 4K inset). Moreover, the lack of change on I_f density upon isoproterenol stimulation reveals a perturbed I_f modulation

by β-AR stimulation in SAN from HFpEF animals (Figure 4L). Although decreased $I_{Ca,L}$ and I_f densities were found in SAN cells from 2-hit HFpEF mice compared to controls (Online Figure XII, A–B), these changes were modest compared to those seen in HFpEF rats.

Compromised intracellular Ca^{2+} transients in HFpEF SAN

Several mechanisms account for the automaticity of pacemaker cells, including the interdependency of the membrane and Ca^{2+} clocks[34], the latter being the intracellular Ca^{2+} release governed by ryanodine receptors and the electrogenic Na^+/Ca^{2+} exchanger (NCX)[11,35]. Thus, we characterized Ca^{2+} transients in SAN cells within the intact tissue loaded with a Ca^{2+} indicator using a high-speed 2D confocal microscopy. Figure 5A represents time-course images of automatic Ca^{2+} transients within the intact SAN. In control, rhythmic Ca^{2+} transients occurred simultaneously throughout the entire SAN (Online Video II). Interesting, even under baseline condition, dysrhythmic cells with Ca^{2+} waves, surrounded by rhythmic cells, were observed in random regions within the primary SAN region from HFpEF (Figure 5B and Online Video III), while β-AR stimulation led to aberrant sinus rhythm only in HFpEF SAN (Online Video IV).

To investigate whether Ca^{2+} handling is affected in the SAN of HFpEF animals, the membrane potential of isolated SAN cells loaded with a Ca^{2+} indicator was voltage-clamped at −60 mV to minimize any contribution of the membrane clock. Triggered action potentials (0 mV square voltage pulses at 1 Hz) demonstrate similar steady-state twitch Ca^{2+} transient amplitude at baseline between groups (Figure 5C–D). Unchanged Ca^{2+} transient amplitude may reflect the role of $Ca_v1.2$ in maintaining the bulk of Ca^{2+} in the SAN, as proposed[36]. Considering that Ca^{2+} handling is affected by a frequency-dependent mechanism[37], and the fact that HFpEF animals have a lower response to isoproterenol, Ca^{2+} transients were assessed at a constant beating rate (Figure 5C–D). Elevation of Ca^{2+} transient amplitude was observed in control SAN upon β-AR stimulation, while no significant change was found in HFpEF SAN cells (Figure 5C–D). Cytosolic Ca^{2+} removal, measured as the Ca^{2+} transient decay time, was similar between groups at baseline (Figure 5E). However, the enhancement of Ca^{2+} reuptake upon β-AR stimulation was only observed in control cells; Ca^{2+} reuptake remained unchanged in HFpEF SAN cells (Figure 5E). We then checked the sarcoplasmic reticulum (SR) Ca^{2+} load and Ca^{2+} extrusion by applying a rapid caffeine-induced Ca^{2+} release, which activates Ca^{2+} extrusion via I_{NCX}. (Figure 5F). No significant changes were observed in the SR Ca^{2+} content (Figure 5G) and I_{NCX} between groups (Figure 5H), as also observed in chronic HF[37,38].

Computational modeling of biophysically-detailed human HFpEF SAN models

Lastly, our experimental findings regarding the membrane clock and Ca^{2+} clock remodeling in HFpEF were integrated into a quantitative human SAN model[39] (Figure 6A). Without isoproterenol, HFpEF SAN models exhibited identical spontaneous action, potential morphology, and beating rate compared to control (Figure 6B). In contrast, all HFpEF models exhibited submaximal beating rate (76 ± 1 vs 94 bpm; Figures 6B and 6C), delayed beating rate response (τ_{on}: 3.6 ± 1.2 vs 1.6 sec), and prolonged beating rate recovery (τ_{off}: 3.2 ± 0.5 vs 1.4 sec) (Figure 6D). Consistent with experimental findings, the increase in

Ca^{2+} transient amplitude of HFpEF models under isoproterenol stimulation was also smaller than that of control (Online Figures XIV, B–C).

Next, we investigated the efficacy of targeting the remodeled membrane versus the Ca^{2+} clock of HFpEF SAN models in ameliorating the chronotropic response (Figures 6E–F). To accomplish this, membrane clock remodeling (MCR) or Ca^{2+} clock remodeling (CCR) of HFpEF SAN models were independently reversed (i.e., returned to control model parameter values). The increase in beating rate under isoproterenol was attenuated in HFpEF SAN models when CCR was targeted compared to when MCR was targeted (1.46 ± 0.21 bpm vs 19.66 ± 0.65 bpm); the beating rate of the control model increased by ~20.2 bpm under isoproterenol. Both τ_{on} and τ_{off} fell to values comparable to that of control in HFpEF SAN models when MCR was targeted. Contrarily, both τon and τoff remained significantly larger in HFpEF SAN models when CCR was targeted (Figure 6F). In summary, targeting MCR in HFpEF SAN models ameliorated all aspects of chronotropic response but targeting CCR did not.

In the prior experiments, we sought to understand what would happen if an aspect of pathophysiological remodeling was reversed. Next, however, we conducted a sensitivity analysis to determine how maximal beating rate under isoproterenol changed with respect to each individual membrane clock and Ca^{2+} clock parameters across all HFpEF SAN models (Figure 6G). We chose to focus on submaximal BR as the presentation of CI to treat because it is one of the standard metrics used to diagnose patients in the clinic[22]. The magnitude and sign of a sensitivity coefficient indicate the degree of change and its correlation between BR and a specific parameter. We found that the parameters k_{dL} (I_{CaL} activation kinetics) and g_f (funny current conductance) had the largest impacts on maximal BR under isoproterenol (0.98 ± 0.02 and 0.15 ± 0.02, respectively). Consistent with our previous simulation results, changes to the membrane clock are associated with changes in maximum beating rate under isoproterenol. Moreover, these results suggest that I_{CaL} would be a particularly promising therapeutic target for treating CI.

Discussion

HFpEF is now regarded as a systemic syndrome that goes beyond left ventricular diastolic dysfunction[2]. Although the pathophysiology of CI associated with exercise intolerance remains uncertain, it is a cardinal feature of human HFpEF. By investigating the mechanisms underlying the limited chronotropic response in HFpEF animal models, we identified SAN dysfunction induced by stress. Our integrated approach revealed evidence of CI in both types of HF (HFrEF and HFpEF), and carefully characterized functional, structural, and molecular features underlying the defective SAN function in HFpEF.

Although autonomic and endothelial dysfunction[1] and lower cardiopulmonary reserve[40] are critical components of exercise intolerance in HFpEF patients, here we expand the current knowledge proposing SAN dysfunction as a new component contributing to the impaired exercise tolerance in HFpEF[3]. Our findings demonstrate impaired CO reserve in HFpEF, which has been shown to be a critical determinant of exercise intolerance in HFpEF patients[41]. Disease-associated SAN dysfunction has been described in many heart

conditions[7–9,42], but has not been examined in HFpEF. Studies in human, canine, and mouse SAN demonstrated that maladaptive structural remodeling in heart disease with SAN dysfunction leads to anatomical obstacles favoring conduction abnormalities[7,23,28]. Moreover, increased SAN fibrosis may create additional insulation layers in the SAN pacemaker complex, which can impair the synchronization of different pacemaker clusters, thereby facilitating multiple leading pacemakers[7,23,28]. Thus, source-sink mismatch and inadequate SAN redundancies essential for protecting heart rhythmicity predispose the SAN dysfunction in HFpEF, by which lethal arrhythmias could occur[18,43]. Supporting the H_2FPEF[44] and HFA-PEFF[45] diagnostic scores, our findings advocate for exercise testing to unmask CI and facilitate HFpEF diagnosis.

Multiple animal models of HFpEF have been developed[46] and faithfully recapitulate critical features of human diseases[14,17,19–21]. Taking into consideration that hypertension is one of the most prevailing risk factors in patients with sick sinus syndrome[47], the remarkable hypertensive feature of the DSS rat HFpEF model coincides with the high prevalence in human HFpEF[2]. This rat model also has insulin resistance and hyperlipidemia[15,16], further increasing its relevance to human HFpEF. Moreover, we recently reported impaired SAN function using a HFpEF model that replicates the chronological development of this disease and the epidemiological evidence of gender-related distribution[48]. In addition, our results were partially replicated in the recently described 2-hit model of HFpEF. Taken together, our findings suggest the CI is a common condition associated with HF, caused by intrinsic SAN dysfunction in HFpEF.

The current view of spontaneous cardiac pacemaking activity relies on the synchronous function of voltage-dependent ion channels (named membrane clock) coupled to a "Ca^{2+} clock", generating highly interdependent and synchronic oscillations[34]. However, the diversity of cell types populating the leading SAN region gives an extra, but decisive, structural complexity that goes beyond its fibrotic insulation. Multiple intranodal pacemakers have different sensitivity to physiologic and pathological stimulations[49], which are fundamental to maintaining SAN robustness, especially during fight-or-flight response needs[23,48]. The co-existence of similar but not identical pacemaker cells within the SAN and surrounding working atrial myocardium has been proposed[25,26,49], and these observations might be justified by differential mRNA cargos of SAN pacemaker cells[29,30]. Although shifts in the molecular signature of SAN towards transitional cells seem not to be responsible for the SAN dysfunction in HFpEF, enrichment of gene clusters related to oxidative stress and inflammation may further amplify the severity of the disease[50,51]. While transcriptome profiling at single-cell resolution has provided a molecular transcriptome atlas of SAN tissue at the embryonic stage[29,30], the challenges imposed by adult stages, such as low and variable yield of viable pacemaker cells, irregular shape, and large cell size represent a technical limitation of the present study.

Given the vital importance of adequate β-AR response, multiple components of the pacemaking machinery exert clear and quantifiable contributions to maintain and/or accelerate the HR, while the loss of these components impairs the proper regulation of rate response[28,34]. Depressed expression and function of the membrane clock components may account for the reduced chronotropic reserve in HFpEF, which has also been linked

with SAN dysfunction in transgenic mice lacking $Ca_v1.3$ or Hcn4[52,53]. The role of Hcn4 channel has been investigated in HFpEF, where it was hypothesized that prolonging diastole can favor complete myocardial relaxation, thereby leading to decreased filling pressures[54]. However, ivabradine, a selective inhibitor of I_f, failed to improve the diastolic function and exercise tolerance in HFpEF[55,56]. Our results further question the rationale for ivabradine in HFpEF. Interestingly, despite the presence of CI in HFrEF, ivabradine has proven to be beneficial in HFrEF patients in the absence of bradycardia[57]. Distinct mechanisms of CI and SAN dysfunction in different forms of HF may account for these differences. Thus, the identification of unique molecular signatures of SAN dysfunction in HFrEF and HFpEF warrants further investigation.

In summary, exercise intolerance and limited chronotropic response in HFpEF are associated with functional, structural, and molecular remodeling of the SAN leading to defective fail-safe mechanisms. Impaired SAN robustness in HFpEF is characterized by reduced chronotropic response to β-AR stimulation and uncoordinated recruitment of pacemaker clusters under stress conditions favoring rhythmic abnormalities.

Limitations and Perspectives

Some limitations of the present study should be noted. First, although we showed concordant findings from two distinct HFpEF models, the limitations of translating the findings to humans were recently discussed[2], supporting the need for improved pre-clinical models. Second, although this study provides granular details of mechanisms responsible for SAN dysfunction, we did not establish a direct link with exercise intolerance. Despite these limitations, the present study brings novel mechanistic insights into SAN dysfunction in HFpEF. Future studies are needed to establish the potential role of novel specific therapies to target this condition.

Supplementary Material

Refer to Web version on PubMed Central for supplementary material.

ACKNOWLEDGMENTS

We thank Eduardo Marbán for numerous helpful discussions, Lisa Trahan for editorial assistance, and Catherine Bresee for statistical consultation.

SOURCES OF FUNDING

This research was supported by National Institutes of Health (grants R01 HL135866, and R01 HL147570 to EC, grants R01 HL142496, R01 HL126802 and U01HL141074 to NT), a Leducq Foundation award to NT, the Peer-Reviewed Medical Research Program of the US Department of Defense (PR150620), American Heart Association (836665 to TM), and the Cedars-Sinai Board of Governors.

Nonstandard Abbreviations and Acronyms

SAN	sinoatrial node
HF	heart failure

HFpEF	heart failure with preserved ejection fraction
HFrEF	heart failure with reduced ejection fraction
CI	chronotropic incompetence
β-AR	Beta-adrenergic receptor

References

1. Borlaug BA, Melenovsky V, Russell SD, et al. Impaired chronotropic and vasodilator reserves limit exercise capacity in patients with heart failure and a preserved ejection fraction. Circulation. 2006;114:2138–2147. [PubMed: 17088459]
2. Shah SJ, Borlaug BA, Kitzman DW, et al. Research Priorities for Heart Failure With Preserved Ejection Fraction: National Heart, Lung, and Blood Institute Working Group Summary. Circulation. 2020;141:1001–1026. [PubMed: 32202936]
3. Sarma S, Stoller D, Hendrix J, et al. Mechanisms of Chronotropic Incompetence in Heart Failure With Preserved Ejection Fraction. Circ Heart Fail. 2020;13:e006331. [PubMed: 32164435]
4. Borlaug BA, Kane GC, Melenovsky V, et al. Abnormal right ventricular-pulmonary artery coupling with exercise in heart failure with preserved ejection fraction. Eur Heart J. 2016;37:3293–3302.
5. Borlaug BA, Nishimura RA, Sorajja P, et al. Exercise hemodynamics enhance diagnosis of early heart failure with preserved ejection fraction. Circ Heart Fail. 2010;3:588–595. [PubMed: 20543134]
6. Del Buono MG, Arena R, Borlaug BA, et al. Exercise Intolerance in Patients With Heart Failure: JACC State-of-the-Art Review. J Am Coll Cardiol. 2019;73:2209–2225. [PubMed: 31047010]
7. Lou Q, Hansen BJ, Fedorenko O, et al. Upregulation of adenosine A1 receptors facilitates sinoatrial node dysfunction in chronic canine heart failure by exacerbating nodal conduction abnormalities revealed by novel dual-sided intramural optical mapping. Circulation. 2014;130:315–324. [PubMed: 24838362]
8. Soltysinska E, Speerschneider T, Winther SV, et al. Sinoatrial node dysfunction induces cardiac arrhythmias in diabetic mice. Cardiovasc Diabetol. 2014;13:122. [PubMed: 25113792]
9. Yanni J, Tellez JO, Maczewski M, et al. Changes in ion channel gene expression underlying heart failure-induced sinoatrial node dysfunction. Circ Heart Fail. 2011;4:496–508. [PubMed: 21565973]
10. Sanders P, Kistler PM, Morton JB, et al. Remodeling of sinus node function in patients with congestive heart failure: reduction in sinus node reserve. Circulation. 2004;110:897–903. [PubMed: 15302799]
11. Cingolani E, Goldhaber JI, Marbán E. Next-generation pacemakers: from small devices to biological pacemakers. Nat Rev Cardiol. 2018;15:139–150. [PubMed: 29143810]
12. John RM, Kumar S. Sinus Node and Atrial Arrhythmias. Circulation. 2016;133:1892–1900. [PubMed: 27166347]
13. Zakeri R, Chamberlain AM, Roger VL, et al. Temporal relationship and prognostic significance of atrial fibrillation in heart failure patients with preserved ejection fraction: a community-based study. Circulation. 2013;128:1085–1093. [PubMed: 23908348]
14. Gallet R, de Couto G, Simsolo E, et al. Cardiosphere-derived cells reverse heart failure with preserved ejection fraction (HFpEF) in rats by decreasing fibrosis and inflammation. JACC Basic Transl Sci. 2016;1:14–28. [PubMed: 27104217]
15. Wendt N, Schulz A, Qadri F, et al. Genetic analysis of salt-sensitive hypertension in Dahl rats reveals a link between cardiac fibrosis and high cholesterol. Cardiovasc Res. 2009;81:618–626. [PubMed: 18824493]
16. Reaven GM, Twersky J, Chang H. Abnormalities of carbohydrate and lipid metabolism in Dahl rats. Hypertens Dallas Tex 1979. 1991;18:630–635.
17. Cho JH, Zhang R, Kilfoil PJ, et al. Delayed Repolarization Underlies Ventricular Arrhythmias in Rats With Heart Failure and Preserved Ejection Fraction. Circulation. 2017;136:2037–2050. [PubMed: 28974519]

18. Cho JH, Zhang R, Aynaszyan S, et al. Ventricular Arrhythmias Underlie Sudden Death in Rats With Heart Failure and Preserved Ejection Fraction. Circ Arrhythm Electrophysiol. 2018;11:e006452. [PubMed: 30030266]
19. Schiattarella GG, Altamirano F, Tong D, et al. Nitrosative stress drives heart failure with preserved ejection fraction. Nature. 2019;568:351–356. [PubMed: 30971818]
20. Tong D, Schiattarella GG, Jiang N, et al. NAD+ Repletion Reverses Heart Failure With Preserved Ejection Fraction. Circ Res. 2021;128:1629–1641. [PubMed: 33882692]
21. Schiattarella GG, Altamirano F, Kim SY, et al. Xbp1s-FoxO1 axis governs lipid accumulation and contractile performance in heart failure with preserved ejection fraction. Nat Commun. 2021;12:1684. [PubMed: 33727534]
22. Zweerink A, van der Lingen A-LCJ, Handoko ML, et al. Chronotropic Incompetence in Chronic Heart Failure. Circ Heart Fail. 2018;11:e004969. [PubMed: 30354566]
23. Li N, Hansen BJ, Csepe TA, et al. Redundant and diverse intranodal pacemakers and conduction pathways protect the human sinoatrial node from failure. Sci Transl Med. 2017;9:eaam5607. [PubMed: 28747516]
24. Ungerer M, Böhm M, Elce JS, et al. Altered expression of beta-adrenergic receptor kinase and beta 1-adrenergic receptors in the failing human heart. Circulation. 1993;87:454–463. [PubMed: 8381058]
25. Boyett MR, Honjo H, Kodama I. The sinoatrial node, a heterogeneous pacemaker structure. Cardiovasc Res. 2000;47:658–687. [PubMed: 10974216]
26. Fedorov VV, Schuessler RB, Hemphill M, et al. Structural and Functional Evidence for Discrete Exit Pathways That Connect the Canine Sinoatrial Node and Atria. Circ Res. 2009;104:915–923. [PubMed: 19246679]
27. Cho JH, Kilfoil PJ, Zhang R, et al. Reverse electrical remodeling in rats with heart failure and preserved ejection fraction. JCI Insight. 2018;3(19):e121123.
28. Glukhov AV, Kalyanasundaram A, Lou Q, et al. Calsequestrin 2 deletion causes sinoatrial node dysfunction and atrial arrhythmias associated with altered sarcoplasmic reticulum calcium cycling and degenerative fibrosis within the mouse atrial pacemaker complex1. Eur Heart J. 2015;36:686–697. [PubMed: 24216388]
29. Goodyer WR, Beyersdorf BM, Paik DT, et al. Transcriptomic Profiling of the Developing Cardiac Conduction System at Single-Cell Resolution. Circ Res. 2019;125:379–397. [PubMed: 31284824]
30. van Eif VWW, Stefanovic S, van Duijvenboden K, et al. Transcriptome analysis of mouse and human sinoatrial node cells reveals a conserved genetic program. Dev Camb Engl. 2019;146(8):dev173161.
31. Mangoni ME, Couette B, Bourinet E, et al. Functional role of L-type Cav1.3 Ca2+ channels in cardiac pacemaker activity. Proc Natl Acad Sci U S A. 2003;100:5543–5548. [PubMed: 12700358]
32. Mangoni ME, Traboulsie A, Leoni A-L, et al. Bradycardia and slowing of the atrioventricular conduction in mice lacking CaV3.1/alpha1G T-type calcium channels. Circ Res. 2006;98:1422–1430. [PubMed: 16690884]
33. Ono K, Iijima T. Pathophysiological significance of T-type Ca2+ channels: properties and functional roles of T-type Ca2+ channels in cardiac pacemaking. J Pharmacol Sci. 2005;99:197–204. [PubMed: 16272791]
34. Tsutsui K, Monfredi OJ, Sirenko-Tagirova SG, et al. A coupled-clock system drives the automaticity of human sinoatrial nodal pacemaker cells. Sci Signal. 2018;11.
35. Torrente AG, Zhang R, Zaini A, et al. Burst pacemaker activity of the sinoatrial node in sodium-calcium exchanger knockout mice. Proc Natl Acad Sci U S A. 2015;112:9769–9774. [PubMed: 26195795]
36. Torrente AG, Fossier L, Baudot M, et al. Role of L-type Cav1.3 Ca2+ channels in Ca2+ handling and SAN pacemaker activity altered by external conditions. Arch Cardiovasc Dis Suppl. 2018;10:241.
37. Verkerk AO, van Borren MMGJ, van Ginneken ACG, et al. Ca(2+) cycling properties are conserved despite bradycardic effects of heart failure in sinoatrial node cells. Front Physiol. 2015;6:18. [PubMed: 25698973]

38. Verkerk AO, Wilders R, Coronel R, et al. Ionic remodeling of sinoatrial node cells by heart failure. Circulation. 2003;108:760–766. [PubMed: 12885752]
39. Fabbri A, Fantini M, Wilders R, et al. Computational analysis of the human sinus node action potential: model development and effects of mutations. J Physiol. 2017;595:2365–2396. [PubMed: 28185290]
40. Gorter TM, Obokata M, Reddy YNV, et al. Exercise unmasks distinct pathophysiologic features in heart failure with preserved ejection fraction and pulmonary vascular disease. Eur Heart J. 2018;39:2825–2835. [PubMed: 29947750]
41. Obokata M, Kane GC, Reddy YNV, et al. Role of Diastolic Stress Testing in the Evaluation for Heart Failure With Preserved Ejection Fraction: A Simultaneous Invasive-Echocardiographic Study. Circulation. 2017;135:825–838. [PubMed: 28039229]
42. Neco P, Torrente A, Mesirca P, et al. Paradoxical Effect of Increased Diastolic Ca2+ Release and Decreased Sinoatrial Node Activity in a Mouse Model of Catecholaminergic Polymorphic Ventricular Tachycardia. Circulation. 2012;126:392–401. [PubMed: 22711277]
43. Vaduganathan M, Patel RB, Michel A, et al. Mode of Death in Heart Failure With Preserved Ejection Fraction. J Am Coll Cardiol. 2017;69:556–569. [PubMed: 28153111]
44. Reddy YNV, Carter RE, Obokata M, et al. A Simple, Evidence-Based Approach to Help Guide Diagnosis of Heart Failure With Preserved Ejection Fraction. Circulation. 2018;138:861–870. [PubMed: 29792299]
45. Pieske B, Tschöpe C, de Boer RA, et al. How to diagnose heart failure with preserved ejection fraction: the HFA-PEFF diagnostic algorithm: a consensus recommendation from the Heart Failure Association (HFA) of the European Society of Cardiology (ESC). Eur J Heart Fail. 2020;22:391–412. [PubMed: 32133741]
46. Valero-Muñoz M, Backman W, Sam F. Murine Models of Heart Failure with Preserved Ejection Fraction: a “Fishing Expedition.” JACC Basic Transl Sci. 2017;2:770–789. [PubMed: 29333506]
47. Jensen PN, Gronroos NN, Chen LY, et al. Incidence of and Risk Factors for Sick Sinus Syndrome in the General Population. J Am Coll Cardiol. 2014;64:531–538. [PubMed: 25104519]
48. Mesquita TRR, Zhang R, de Couto G, et al. Mechanisms of atrial fibrillation in aged rats with heart failure with preserved ejection fraction. Heart Rhythm. 2020;17:1025–1033. [PubMed: 32068183]
49. Kim MS, Maltsev AV, Monfredi O, et al. Heterogeneity of calcium clock functions in dormant, dysrhythmically and rhythmically firing single pacemaker cells isolated from SA node. Cell Calcium. 2018;74:168–179. [PubMed: 30092494]
50. Swaminathan PD, Purohit A, Soni S, et al. Oxidized CaMKII causes cardiac sinus node dysfunction in mice. J Clin Invest. 2011;121:3277–3288. [PubMed: 21785215]
51. Leuschner F, Nahrendorf M. Novel functions of macrophages in the heart: insights into electrical conduction, stress, and diastolic dysfunction. Eur Heart J. 2020;41:989–994. [PubMed: 30945736]
52. Baruscotti M, Bucchi A, Viscomi C, et al. Deep bradycardia and heart block caused by inducible cardiac-specific knockout of the pacemaker channel gene Hcn4. Proc Natl Acad Sci U S A. 2011;108:1705–1710. [PubMed: 21220308]
53. Platzer J, Engel J, Schrott-Fischer A, et al. Congenital deafness and sinoatrial node dysfunction in mice lacking class D L-type Ca2+ channels. Cell. 2000;102:89–97. [PubMed: 10929716]
54. Reil J-C, Hohl M, Reil G-H, et al. Heart rate reduction by If-inhibition improves vascular stiffness and left ventricular systolic and diastolic function in a mouse model of heart failure with preserved ejection fraction. Eur Heart J. 2013;34:2839–2849. [PubMed: 22833515]
55. Pal N, Sivaswamy N, Mahmod M, et al. Effect of Selective Heart Rate Slowing in Heart Failure With Preserved Ejection Fraction. Circulation. 2015;132:1719–1725. [PubMed: 26338956]
56. Komajda M, Isnard R, Cohen-Solal A, et al. Effect of ivabradine in patients with heart failure with preserved ejection fraction: the EDIFY randomized placebo-controlled trial. Eur J Heart Fail. 2017;19:1495–1503. [PubMed: 28462519]
57. Bouabdallaoui N, O’Meara E, Bernier V, et al. Beneficial effects of ivabradine in patients with heart failure, low ejection fraction, and heart rate above 77 b.p.m. ESC Heart Fail. 2019;6:1199–1207. [PubMed: 31591826]

58. Elkholey K, Morris L, Niewiadomska M, et al. Sex differences in the incidence and mode of death in rats with heart failure with preserved ejection fraction. Exp Physiol. 2021;106:673–682. [PubMed: 33428276]

59. Tong D, Schiattarella GG, Jiang N, et al. Female Sex Is Protective in a Preclinical Model of Heart Failure With Preserved Ejection Fraction. Circulation. 2019;140:1769–1771. [PubMed: 31738599]

60. Laughner JI, Ng FS, Sulkin MS, et al. Processing and analysis of cardiac optical mapping data obtained with potentiometric dyes. Am J Physiol Heart Circ Physiol. 2012;303:H753–765. [PubMed: 22821993]

61. Lagarias JC, Reeds JA, Wright MH, et al. Convergence Properties of the Nelder--Mead Simplex Method in Low Dimensions. SIAM J Optim. 1998;9:112–147.

62. Severi S, Fantini M, Charawi LA, et al. An updated computational model of rabbit sinoatrial action potential to investigate the mechanisms of heart rate modulation. J Physiol. 2012;590:4483–4499. [PubMed: 22711956]

Clinical Perspective

What is new?

- We identified latent SAN dysfunction in HFpEF, that can be unmasked under stress testing.
- Our integrated approach revealed functional, structural, and molecular features underlying the defective SAN function in HFpEF.
- Although transcriptomic profiling reveals changes in multiple disease-associated genes, depressed “membrane clock” and “Ca^{2+} clock” components are closely linked to the impaired SAN function.

What are the clinical implications?

- Provocative testing can be valuable to elicit functional abnormalities to facilitate HFpEF diagnosis.
- Considering the exceptionally high clinical and epidemiological convergence between atrial fibrillation and HFpEF, SAN dysfunction may underlie the development of abnormal atrial rhythms in HFpEF.

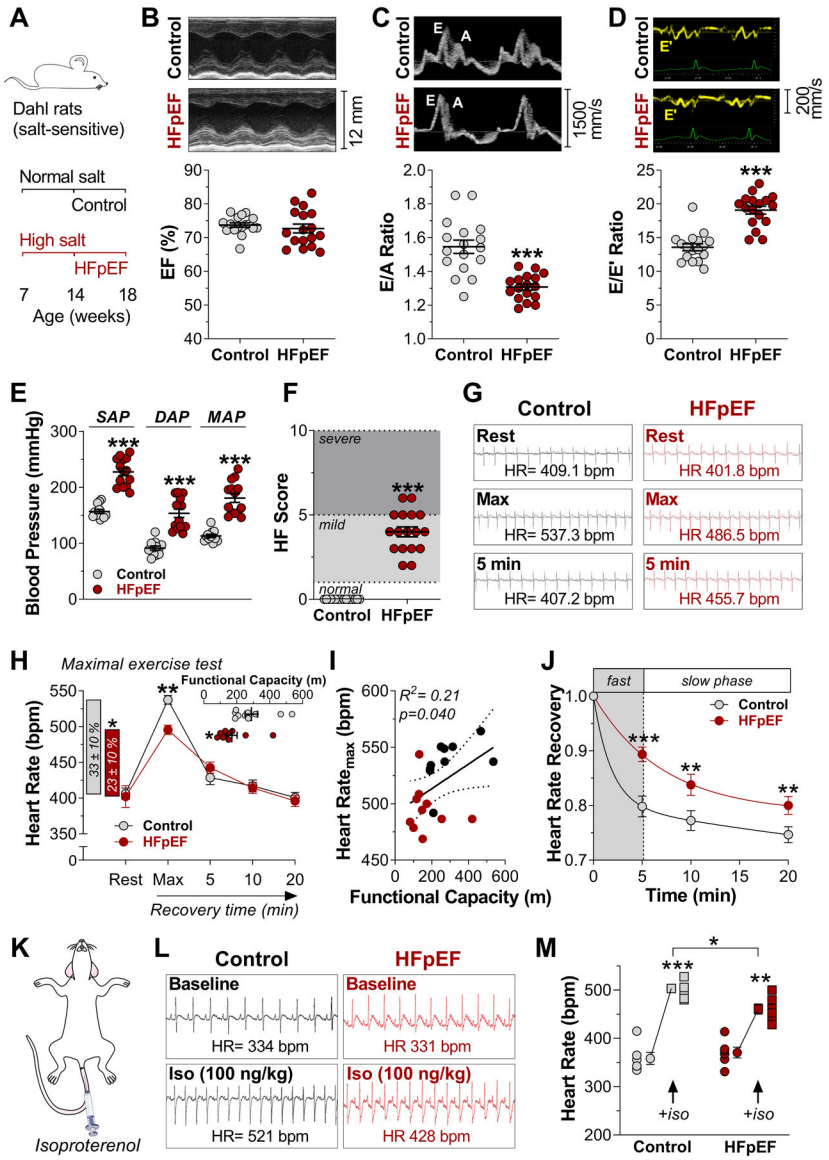

Figure 1. Cardinal exercise intolerance and chronotropic incompetence of HFpEF phenotyping are associated with lower β-AR responsiveness.

A: Experimental design. Dahl salt-sensitive rats were maintained on a normal salt (0.4%) or high salt (8%) dietary regimens from 7 weeks of age and HFpEF verified between 14–18 weeks old. **B:** Representative left ventricular M-mode echocardiographic images (*top*) of ejection fraction (EF) analysis (*bottom*). **C:** Representative images (*top*) of pulse-wave Doppler showing E (early filling)– and A (atrial filling)–wave changes (*bottom*). **D:** Representative images (*top*) of tissue Doppler describing E′- and A′-wave changes (*bottom*). **E:** Noninvasive blood pressure measurements. DAP = diastolic arterial pressure; MAP = mean arterial pressure; SAP = systolic arterial pressure. **F:** Heart failure (HF) score defined by the following parameters: appearance, breathing, mobility, edema, and weight. **G:** Representative telemetry ECG recordings. **H:** Resting, maximal, and recovery of heart rate in response to exercise test (inset, functional capacity measured as the total running distance). n = 10 animals in each group. **I:** Relationship between functional capacity and

maximal heart rate response (Pearson coefficient). Data are fit by linear regression; dashed lines represent 95% confidence. **J:** Heart rate recovery time after the maximal exercise test, data are fit by two exponential decay. **K:** *In vivo* isoproterenol (Iso) stress testing was used to determine the chronotropic reserve. **L:** Representative ECG recordings. **M:** Quantification of β-adrenergic–induced heart rate (HR) increase. Data are expressed as mean ± SEM. Unpaired Student *t*-test (B-F, and H insets). RM-ANOVA followed by Bonferroni post hoc test (H, J, and M). $*P < .05$, $**P < .01$, and $***P < .001$.

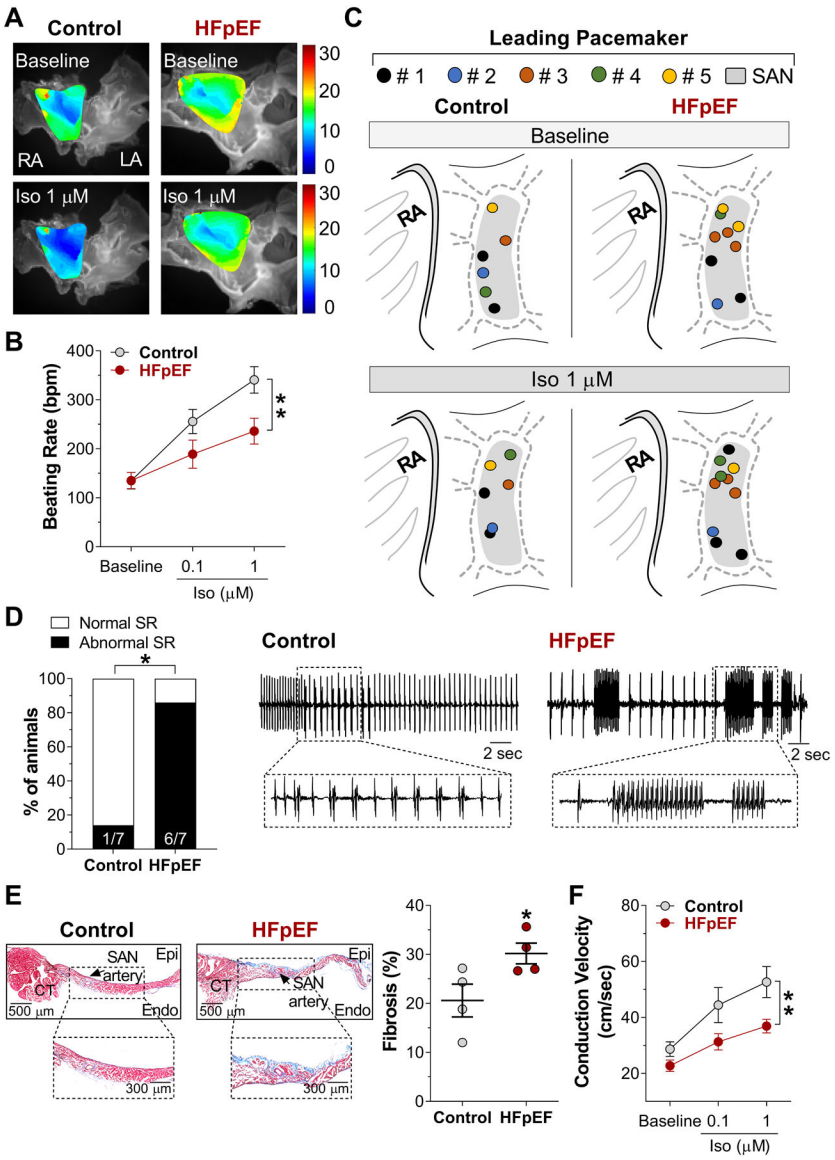

Figure 2. Impaired SAN β-AR responsiveness reveals uncoordinated recruitment of pacemaker clusters favoring rhythmic abnormalities.

A: Representative images of isochronal voltage maps under spontaneous sinus rhythm and isoproterenol stimulation. **B:** Spontaneous sinus rhythm and concentration-response curve for isoproterenol (Iso) were used to evaluate *ex vivo* beating rate. N = 7 animals in each group. **C:** Locations of the SAN leading pacemaker (dots), defined as the earliest activation site and the effects of β-adrenergic stimulation on the leading pacemaker site location. Each colored dot represents an estimated location from 5-sec recordings from an animal replicate replotted onto a schematic SAN region. **D:** Occurrence of abnormal sinus rhythm (SR) throughout the dose-response curve to Iso (*left*) and representative electrogram traces (*right*). **E:** Representative Masson's trichrome–stained sections of SAN (*left*, CT = crista terminalis, Epi= epicardium, and Endo= endocardium) and quantification (*right*). **F:** Conduction velocity within the SAN region at spontaneous sinus rhythm and concentration-response curve for Iso. Data are expressed as mean ± SEM. Statistical significance was

determined using RM-ANOVA followed by Bonferroni post hoc test (B and F). Fisher's exact test (D). Unpaired Student *t*-test (E). **P* < .05 and ***P* < .01.

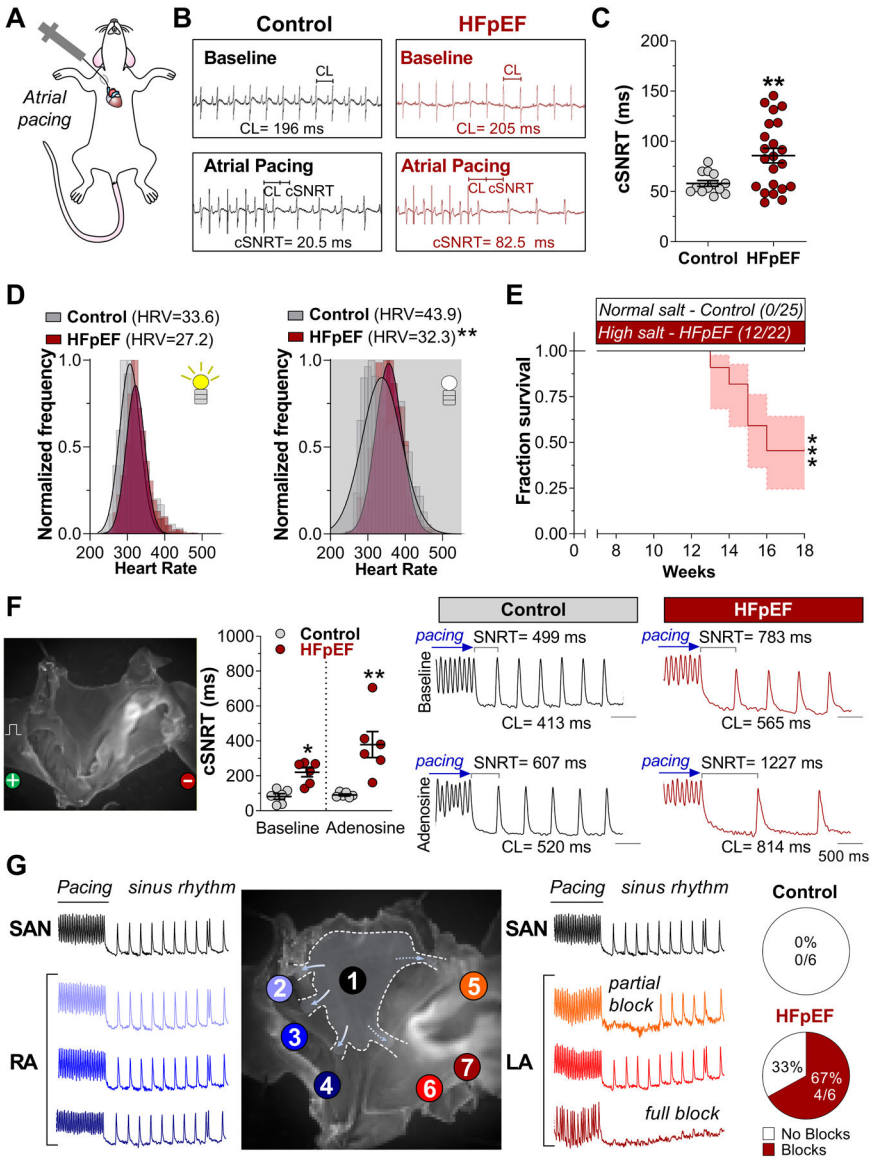

Figure 3. Unmasked SAN dysfunction by adenosine challenge reveals conduction block.

A: Intracardiac electrophysiology study was used to determine the SAN function. Representative ECG recordings (**B**) and quantification of corrected SAN recovery time (cSNRT, corrected by intrinsic CL= cycle length) (**C**). **D:** Histogram of the circadian oscillation of heart rate during day (*left*) and night (*right*). Individual standard derivation of heart rate was used as a measure of heart rate variability (HRV). N = 10 animals in each group. **E:** Survival analysis of control and HFpEF rats until 18 weeks of age. **F:** Representative image of electrodes placement surrounding the *ex vivo* SAN/atrial tissue loaded with a voltage-sensitive dye (*left*). Overdriving suppression of SAN for assessing the cSNRT was achieved by rapid pacing from the right atrium (RA). cSNRT was quantified before (baseline) and after treatment with adenosine (1 μM) for 10 min (*middle*). Representative optical action potential traces during RA pacing and time taken to recover the sinus rhythm (*right*). **G:** Overview of HFpEF SAN maps uncover the presence of conduction

blocks. Data are expressed as mean ± SEM. Unpaired Student *t*-test (C and D). Log-rank test (E). RM-ANOVA followed by Bonferroni post hoc test (F). Fisher's exact test (G). **P* < .05,***P* < .01, and ****P* < .001.

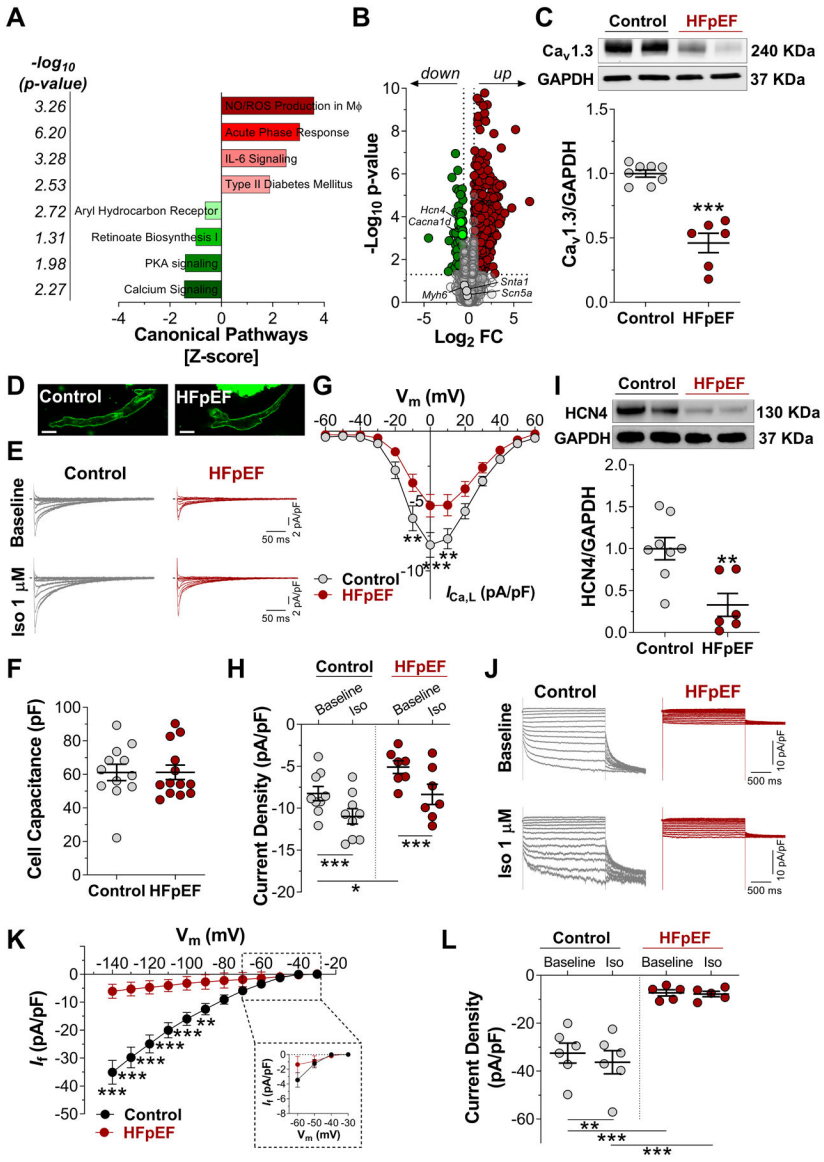

Figure 4. Transcriptome profiling of HFpEF SAN identifies multiple disease-associated mechanisms underpinning depressed membrane clock.

A: Enriched upregulated and downregulated canonical pathways. **B:** Volcano plot of fold change relative to control SAN. Highlighted genes indicate the potential genes related to human sick sinus syndrome, as predicted by *in silico* analysis. N = 4 samples each group. **C:** Representative western blot images (*top*) and quantification of $Ca_v1.3$ (encoded by *Cacna1d*) protein expression (*bottom*). **D:** Representative isolated SAN cells loaded with the voltage dye show the typical spindle shape of pacemaker cells with absent T-tubules (scale bar = 10 µm). **E:** Representative L-type Ca^{2+} channel currents recorded in isolated SAN cells. **F:** cell capacitance. **G:** Average peak current density–voltage relationship of $I_{Ca,L}$ in control (n= 9 cells from 3 animals) and HFpEF (n= 7 cells from 3 animals); **H:** Peak current at 0 mV in the absence or presence of isoproterenol (Iso, 1 µM). **I:** Representative western blot images (*top*) and quantification of Hcn4 protein expression (*bottom*). **J:** Representative time courses of I_f funny current recorded in isolated SAN cells. **K.** Average peak current

density-voltage relationship of I_f in control (n= 6 cells from 3 animals) and HFpEF (n= 5 cells from 3 animals) (*bottom*), inset highlights no difference in I_f current density between −60 to −30 mV. **L:** Peak current at −140 mV in the absence or presence of isoproterenol (Iso, 1 μM). Data are expressed as mean ± SEM. Statistical significance was determined using unpaired Student's *t*-test (C, I, and F). Mixed-effect model with Bonferroni's post hoc test (G). RM-ANOVA followed by Bonferroni post hoc test (H, K, and L). *$P < .05$, **$P < .01$, and ***$P < .001$.

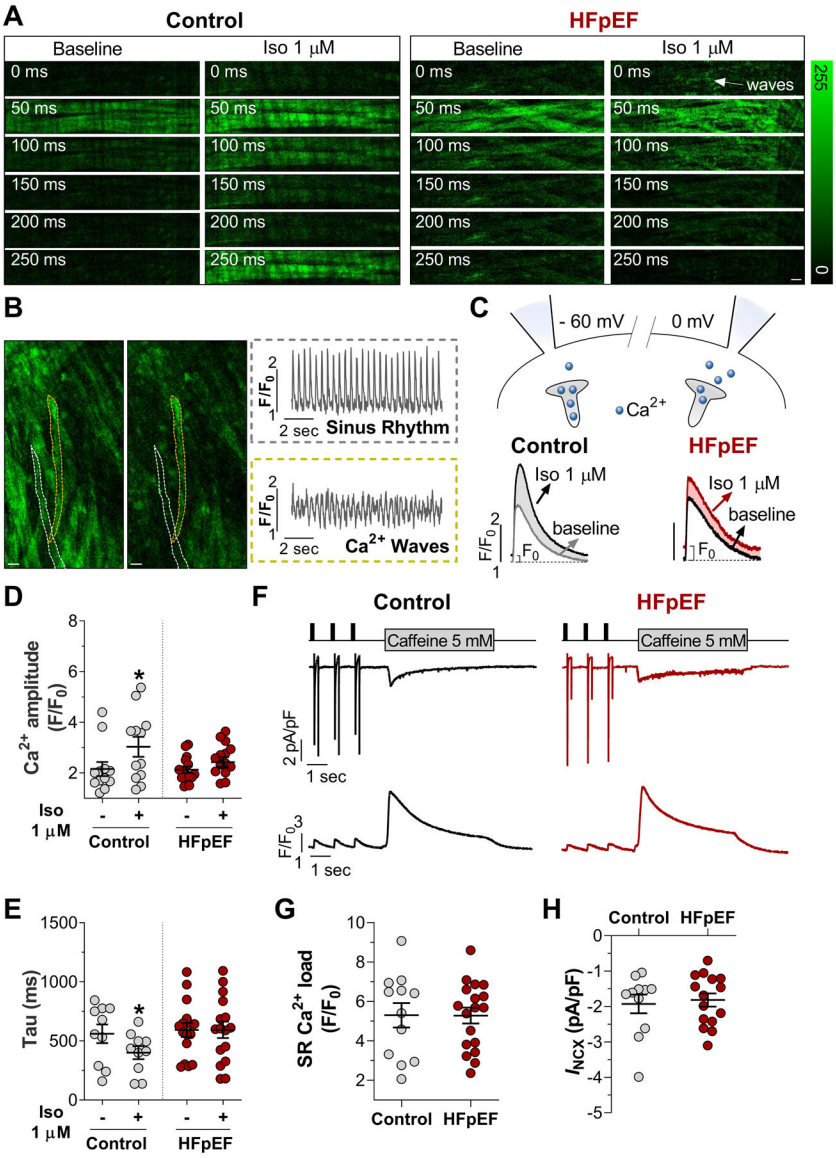

Figure 5. Compromised intracellular Ca^{2+} transients in SAN of HFpEF.

A: Time series of 2D confocal images of pacemaker cells within the intact SAN (scale bar = 60 μm). **B:** A still frame from a 2D confocal image of Ca^{2+} fluorescence in a wide field of the explanted HFpEF SAN tissue, showing two neighbor cells, one under intrinsic sinus rhythm (marked by white dashed lines) and another with Ca^{2+} waves (marked by yellow dashed lines), scale bar = 20 μm. The right panel shows the differential oscillatory pattern. **C:** Membrane depolarization-induced global cytosolic Ca^{2+} transient (*top*) and representative Ca^{2+} transient in control and HFpEF SAN cells under baseline and isoproterenol (Iso) stimulation (*bottom*). **D:** Mean Ca^{2+} transient amplitude. **E:** Mean time constant of Ca^{2+} decay (Tau). **F:** Representative tracings of application of a caffeine solution after pacing to steady state at 1 Hz provided a measurement of caffeine-induced inward NCX current and sarcoplasmic reticulum (SR) load. **G:** Mean SR Ca^{2+} load. **H:** Mean peak NCX current (I_{NCX}). Mean values were obtained from control (n=10–12 cells from 3

animals) and HFpEF (n=15–18 cells from 3 animals). Data are expressed as mean ± SEM. Statistical significance was determined using RM-ANOVA followed by Bonferroni post hoc test (D and E) or unpaired Student's *t*-test (G and H). **P* < .05.

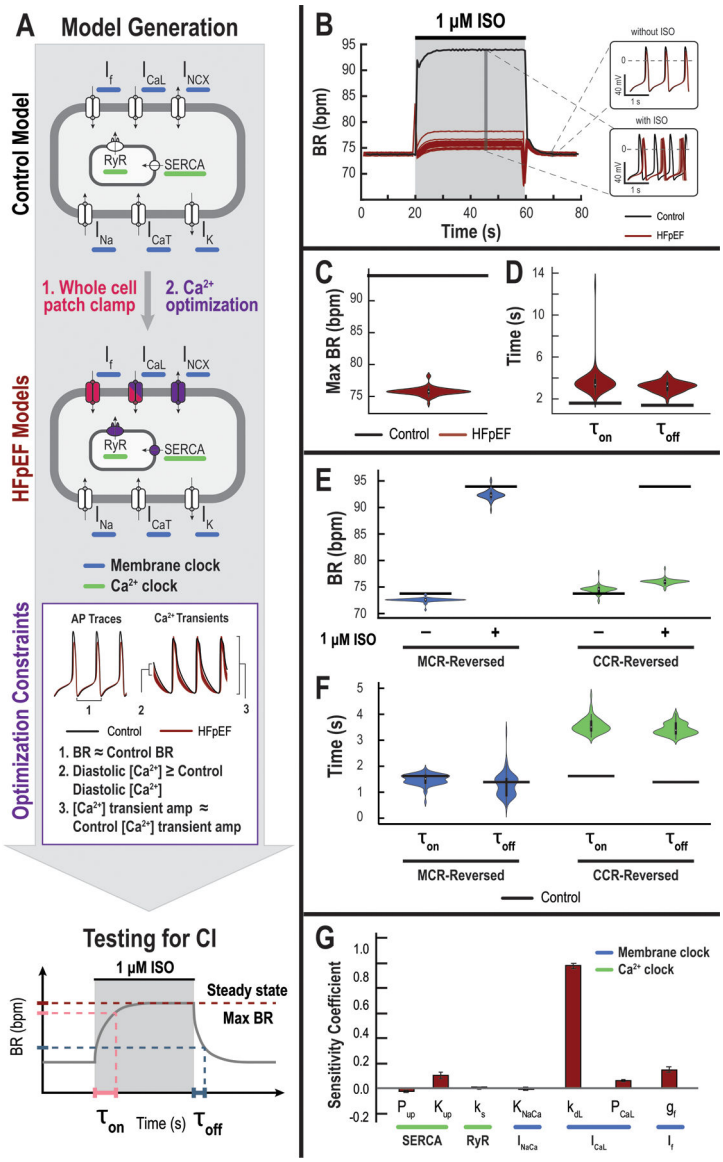

Figure 6. Computer simulations reveal the dominant role of HFpEF-associated membrane clock remodeling on the impaired SAN β-AR responsiveness.

A: Computer simulation workflow. Incorporation of ionic remodeling into biophysically-detailed human SAN membrane kinetic model (top). First, ionic remodeling of the membrane clock (MC: 80% and 34% reduction in funny current and L-type Ca^{2+} current conductances) was incorporated (pink). Subsequently, additional Ca^{2+} handling parameters (SERCA, RyR, L-type Ca^{2+}) were tuned so that the resultant HFpEF models recapitulated changes in experimental Ca^{2+} transient dynamics. When testing for CI (bottom), models were challenged with a 40-sec pulse of 1 μM isoproterenol (ISO); maximal beating rate (BR), BR response (τ_{on}), and BR recovery (τ_{off}) were quantified. **B:** Instantaneous BR plotted versus time for control (black) and HFpEF (red) models subject to a 40-sec 1 μM ISO pulse; representative action potentials (left) for control (black) and collection of HFpEF (red) SAN models with and without ISO (inset). Violin plots of (**C**) maximum BRs, and (**D**) BR response (τ_{on}, left), and BR recovery (τ_{off}, right) of HFpEF models subject to 1 μM ISO

pulse; black horizontal lines indicate corresponding control values. **E and F:** Contributions of MC and CC remodeling to CI. **E:** Steady-state BRs with and without ISO. **F:** BR response (τ_{on}, left) and BR recovery (τ_{off}, right) of models with either MC remodeling (blue) or CC remodeling (green); horizontal black bars indicate control model dynamics. **G:** Bar graph of sensitivity coefficients of membrane and calcium clock parameters. The sensitivity coefficients represent how changes in each of these parameters affect BR.